Molecular and Cellular Targets of the MRI Contrast Agent P947 for Atherosclerosis Imaging

Tanja Ouimet,[†] Eric Lancelot,[‡] Fabien Hyafil,[§] Mario Rienzo,[||] François Deux,[⊥] Marjorie Lemaître,[‡] Sophie Duquesnoy,[†] Jérome Garot,[#] Bernard P. Roques,[†] Jean-Baptiste Michel,[∇] Claire Corot,[‡] and Sébastien Ballet*,[‡]

[†]Pharmaleads, 11 rue Watt, 75013 Paris, France

[‡]Guerbet, Research Center, 16-24 rue Jean Chaptal, 93600 Aulnay-sous-Bois, France

[§]Service de Médecine Nucléaire, AP-HP, Groupe Hospitalier Bichat-Claude Bernard, Université Paris Diderot, Sorbonne Paris Cité, Paris, France

[||]INSERM U955, Physiopathologie et pharmacologie des insuffisances coronaire et cardiaque, Hôpital Henri Mondor, 51 avenue du Maréchal de Lattre de Tassigny, 94000 Créteil, France

[⊥]CNRS UMR 7054, Service de Radiologie, Hôpital Henri Mondor, 51 avenue du Maréchal de Lattre de Tassigny, 94000 Créteil, France

[#]INSERM U955, Physiopathologie et pharmacologie des insuffisances coronaire et cardiaque, Service de Cardiologie, Hôpital Henri Mondor, 51 avenue du Maréchal de Lattre de Tassigny, 94000 Créteil, France

[∇]INSERM U698, Hémostase, Bio-ingénierie et Remodelage Cardio-Vasculaire, Hôpital Bichat, 46 rue Henri Huchard, 75018 Paris, France

S *Supporting Information*

ABSTRACT: P947 (DOTA-Gd-peptide) was recently identified as an MRI contrast agent for the detection and characterization of the matrix metalloproteinases (MMP)-rich atherosclerotic plaques. Because this product displays a broad spectrum affinity for the MMP family, we hypothesized that it may also recognize other metalloproteinases over-activated in vulnerable atherosclerotic plaques. Therefore, this study aimed at describing, at the molecular and cellular level, the interactions between P947 and proteases of atherosclerotic plaques. Fluorimetric assays were used to measure the *in vitro* affinity of P947 toward recombinant and purified MMPs, angiotensin-converting enzyme (ACE), endothelin-converting enzyme (ECE-1), neutral endopeptidase (NEP), and both aminopeptidases A and N (APA and APN). Using similar fluorimetric assays associated with specific substrates, enzymatic activities were measured in vulnerable and stable plaques collected from human atherosclerotic carotid arteries. *Ex vivo* affinity of P947 for metalloproteinases in vulnerable lesions was subsequently determined. Interaction between P947 and major cell types present in atherosclerotic plaques was also investigated in different cell lines: PMA-1-differentiated THP-1 (macrophage), Ox-LDL-treated THP-1 (foam cell), Jurkat cell line (lymphocyte), and human umbilical vein endothelial cell (HUVEC, endothelial cell). Molecular targeting of P947 was confirmed by fluorimetry, ICP-MS, and *in vitro* MRI approaches. Potential application of P947 for detecting atherosclerotic plaques by *in vivo* MRI was tested in a rabbit model of atherosclerosis. *In vitro*, P947 displayed affinities for purified MMPs, ACE, ECE-1, NEP, APA, and APN in the micromolar range. Interestingly, MMPs, ACE, and APN exhibited higher activities in vulnerable plaques from human atherosclerotic carotid samples, as compared to stable plaques. ECE-1, NEP, and APA had either no activity or the same low activity in both vulnerable and stable plaques. P947 showed micromolar affinities for MMPs, ACE, and APN secreted by plaque samples. Moreover, P947 bound to THP-1 macrophages and THP-1 foam cells in a concentration-dependent manner and with a higher intensity than the control contrast agents DOTA-Gd or P1135 (DOTA-Gd coupled to a scrambled peptide). In THP-1 macrophages, P947 inhibited largely (70%) and almost

continued...
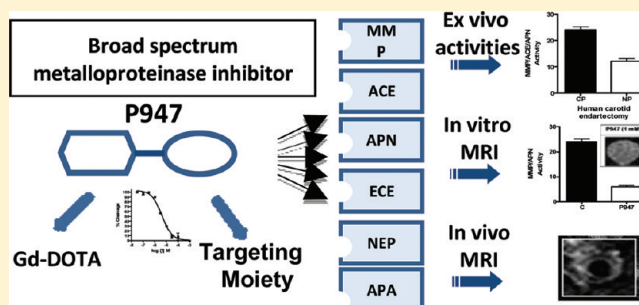
completely (95%) MMP and APN activities, respectively, which strongly suggested an MMP- and APN-dependent binding of P947 to these cells. This enzyme-specific binding was confirmed with *in vitro* MRI. Indeed, the $T1$ value of THP-1 cells decreased from 2.094 s (macrophages w/o P947) to 2.004 s (macrophages with 1 mM of P947). In addition, the Gd content measured by ICP-MS was 11.01 ± 1.05 fg Gd/macrophage when cells were incubated in the presence of P947 and only 5.18 ± 0.43 fg Gd/macrophage with the control product P1135. The difference of Gd concentration between both contrast agents corresponded to a specific accumulation of 5.83 fg Gd/cell, which may be detected by MRI. MR imaging in the atherosclerosis rabbit model showed enhancement of the aortic wall after P947 injection with a significant increase of CNR values from 0.21 ± 0.02 (before injection) to 0.37 ± 0.07 (after injection), demonstrating the efficacy of the contrast agent to detect the atherosclerotic plaques *in vivo*. Taken together, these data suggest that P947 may be an interesting contrast agent for *in vivo* molecular MR imaging of MMPs, ACE, and APN activities present in vulnerable atherosclerotic plaques.

KEYWORDS: *P947, metalloproteinases, macrophage, atherosclerosis, MRI, molecular imaging, atherosclerotic rabbit model*

1. INTRODUCTION

Although vascular remodeling is an important determinant in many physiological processes, it is also observed in vascular pathologies.[1,2] Changes in both cellular and noncellular components are critical for remodeling of the vascular wall. Depending on the pathological process, smooth muscle cell (SMC) growth and migration, endothelial cell (EC) dysfunction, inflammatory cell infiltration, extracellular matrix degradation, or synthesis can occur.

Atherosclerosis is a complex, progressive disease of the large arteries and the leading cause of death in the Western world. Recent research has shown the crucial role of leukocytes in the development and progression of atherosclerotic lesions.[3] Immune cells are already present in early lesions, and advanced plaques show large lipid cores in which macrophages are often present. Recent evidence has revealed considerable diversity in the monocyte and macrophage populations present in the atherosclerotic plaques. The impact of the different macrophage phenotypes (e.g., M1 and M2) in plaque progression and instability is just beginning to be investigated.[4]

Cell migration and tissue remodeling require degradation of the extracellular matrix (ECM). Matrix metalloproteinases (MMPs) are a family of more than 20 structurally related proteases that share the necessity of a Zn^{2+} ion at the catalytic site.[5] All members of the MMP family degrade components of the ECM. They are all synthesized as inactive prepro-enzymes and secreted as latent pro-enzymes requiring activation. The MMP family of enzymes can be divided into four major subclasses, three of which are secreted soluble enzymes and one which is membrane bound exoproteases, referred to as membrane-type MMPs or MT-MMPs. Many human and animal studies have demonstrated up-regulated activities of these enzymes within atherosclerotic lesions, particularly in macrophages, which have been proposed to contribute to plaque rupture.[6,7]

Angiotensin-converting enzyme (ACE) is an ecto-metalloprotease with dipeptidyl-carboxipeptidase activity, playing a key role in the rennin-angiotensin system, generating the bioactive octapeptide angiotensin II (Ang II) by limited proteolysis of its precursor, the Angiotensin I (Ang I) decapeptide. Ang II is a potent vasoconstrictor, but it also accelerates atherogenesis by stimulating SMC proliferation, platelet activation, and cholesterol accumulation in arterial macrophages.[8−11] Hence, Ang II is considered as a regulatory factor in the changes in wall structure and function during vascular remodeling. ACE is abundantly expressed in human atherosclerotic lesions and is localized at the surface of macrophage foam cells, lymphocytes, endothelial cells of neovessels, and spindle-shaped smooth muscle cells.[12−15] There is also important shedding of the enzyme, as evidenced by

the presence of a soluble ACE enzymatic activity in plasma. Other structurally related metalloproteases of the secretory pathway, known for their involvement in peptide homeostasis, are also expressed in these tissues, and together they could play still unexplored functions in these diseases.

Coronary angiography is used in clinical practice to detect severe stenoses associated with chronic myocardial ischemia. Acute coronary syndromes are often caused by the sudden rupture of atherosclerotic plaques, which trigger arterial thrombosis. Ruptured atherosclerotic plaques are characterized by their biological content rather than by the severity of stenosis that they cause. Early detection of vulnerable plaques, at risk of rupture, could help to identify subjects at higher risk of cardiovascular events. New and experimental imaging techniques are being developed to allow for better characterization of atherosclerotic plaques. Molecular imaging based on MRI represents a promising modality to identify vulnerable atherosclerotic plaques., Culprit atherosclerotic plaques are characterized by an intense inflammatory infiltrate and high MMP activity, which could play a key role in plaque rupture. We previously demonstrated the efficacy of a novel contrast agent, P947, for the *in vivo* detection of MMP-rich atherosclerotic lesions using MRI in apolipoprotein E-deficient mice.[16] The P947 molecule consists of a broad-spectrum hydroxamate-type MMP inhibitor to a DOTA contrast agent, thus targeting all MMPs showing an affinity for the inhibitory moiety.

In this study, we investigated the molecular and cellular mechanisms involved in P947 accumulation in atherosclerotic plaques using *in vitro*, *ex vivo*, and *in vivo* approaches. Expression of several metalloproteinases known for their involvement in atherosclerosis (e.g., MMPs, ACE, endothelin converting enzyme) or for which a role is still to be elucidated (neutral endopeptidase, aminopeptidases A and N) was measured in both stable and vulnerable human atherosclerotic carotid plaques. Binding affinities of P947 toward herein identified up-regulated metalloproteinases in vulnerable, culprit plaques were then measured using both recombinant enzymes (*in vitro*) and conditioned media from human atherosclerotic plaque samples (*ex vivo*) by fluorimetric approaches. We measured (ICP-MS) and imaged (MRI) the P947 labeling intensity of cells playing key roles in the vascular remodeling during an atherosclerotic process, i.e. macrophages, foam cells, endothelial cells, and T lymphocytes. Finally, we confirmed the ability of P947 to detect atherosclerotic plaques *in vivo* by MRI in a rabbit model of atherosclerosis.

2. EXPERIMENTAL SECTION

2.1. Materials. P947 (active product) was obtained by coupling an MMP inhibitor to the gadolinium (Gd) chelate,

1,4,7,10-tetraazacyclododecane-*N*,*N'*,*N''*,*N'''*-tetraacetic acid (DOTA), as previously described.[16] P947 has a molecular weight of 1210 Da and an r1 relaxivity value of 5.5 s^{-1}·mM^{-1} in water at 1.5 T and 37 °C. Gd-DOTA (Dotarem), a standard nonspecific gadolinium contrast agent with an r1 relaxivity value of 3.7 s^{-1}·mM^{-1}, and P1135 (inactive product), a Gd-DOTA functionalized with a scrambled MMP inhibitor peptide derived from P947 and an r1 relaxivity value of 6.0 s^{-1}·mM^{-1} in water at 1.5 T and 37 °C, were used as references.

Human purified MMPs (MMP-1, -2, -3, -8, -9, -13, -14) were purchased from Calbiochem (France). Soluble recombinant human ECE-1 (Gln 90−Trp 770, R&D Systems, Lille, France) was reconstituted in 25 mM Tris 100 mM pH 8.0, 150 mM NaCl at 0.1 mg/mL. APN purified from hog kidney was purchased from Perbio Science (Brebières, France) while human recombinant APA (residues 41−957) was from R&D Systems (Lille, France). NEP was purified to homogeneity from rabbit kidney as previously described.[17] The ACE metalloprotease was purified from rat testis as described by Piquilloud and colleagues.[18] The purity of the preparations was verified by SDS-PAGE and coomassie staining, and the enzyme concentrations were determined by densitometry using a BSA scale and the Quantity One program of BioRad. The NEP stock solution was at a concentration of 750 μg/mL while ACE was at 25.3 μg/mL. The fluorigenic APN substrate Ala-β-naphtylamide was purchased from Sigma (France) while the Glu-AMC APA substrate was from Bachem (Weil am Rhein, Germany). The fluorigenic substrates of NEP, ACE, and ECE were synthesized using peptide Fmoc chemistry, as previously described.[19,20] The EDTA and phosphoramidon metalloprotease inhibitors were purchased from Sigma.

RPMI-1640 medium and fetal calf serum (FCS) were purchased from Gibco (Invitrogen, France), and HUVEC package medium was from Lonza (France). Purified mouse FITC-conjugated monoclonal antihuman CD-14 antibody and mouse nonspecific FITC-conjugated IgG (negative control) were purchased from Abcys (France) while the annexin V-FITC/PI kit was from Bender Medsystems (Austria). Purified human oxidized (Ox)-LDL was purchased from Intracell (USA), and Oil-Red-O was purchased from Sigma (France).

2.2. *In Vitro* Inhibitory Potency of P947 against MMPs and Other Metalloproteinases. The inhibitory potency of P947 and P1135 was studied *in vitro* against human MMP-1, -2, -3, -8, -9, -13, and -14. MMPs were used as recommended by the manufacturer, i.e. preincubated for 10 min at 37 °C in Tris 25 mM pH 7.5, CaCl$_2$ 10 mM, NaCl 0.2 M, Brij 0.05% with increasing concentrations of P947 (from 10^{-9} to 10^{-4} M). The reaction was initiated by the addition of 50 μM of the nonselective substrate 7-methoxycoumarin-4-acetyl-Pro-Leu-Gly-Leu-β-(2−4-dinitrophenyl)-L-2.3-diaminopropionyl-Ala-Arg-NH$_2$ (Sigma, France) and left to proceed for 30 min at 37 °C in a final volume of 100 μL. The inhibitory potency of P947 was also tested in the same manner against NEP, ACE, ECE-1, APN, and APA. For ACE (10 ng/mL) a Tris 50 mM pH 8.0, 1% NaCl buffer was used, whereas NEP (200 ng/mL) and ECE-1 (10 μg/mL) activities were monitored in Tris 50 mM pH 7.4 and Tris 100 mM pH 6.8, respectively. While the inhibitory potency of P947 against APN (6.6 mU/mL) was investigated in Tris 50 mM pH 7.4, that against APA (20 ng/mL) was studied in Tris 25 mM pH 8.0, CaCl$_2$ 50 mM, NaCl 0.2 M. For each related metalloproteinase, the inhibitory potency of P947 was studied using a specific fluorigenic substrate as well as a specific and/or high affinity inhibitor as a

positive control i.e. thiorphan for NEP, captopril for ACE, phosphoramidon for ECE-1, RB3014 for APN, and EC33 for APA. Substrate hydrolysis was monitored on a multiwell plate-reader fluorimeter (Berthold Series Twinkle LB 970 coupled to Mikrowin 2000 software) with excitation at 340 nm, emission at 405 nm, and lamp energy at 10 000. Samples with 0% hydrolysis were obtained by adding the substrate to the buffer, and samples with 100% relative activity were prepared without the inhibitor. The cleavage percentage was evaluated and compared with 100% relative activity, and the IC$_{50}$ values were determined accordingly using Graph Pad PRISM software. The K_i values of the inhibitors (mean of at least two independent assays in duplicate) were calculated using the Cheng and Prussoff equation $K_i = IC_{50}/(1 + [S]/K_m)$, where IC$_{50}$ is the concentration yielding fifty percent inhibition of metalloproteinase activity, [S] is the substrate concentration, and K_m is the Michaelis constant.

2.3. Human Carotid Atherorombotic Plaques. Fresh human carotid artery specimens were collected from atherosclerotic patients undergoing carotid endarterectomy in accordance with ethical committee ascent and with patient consent. The culprit region (CP), the stenosic plaque lesion for which the patient had been operated, at the origin of the internal carotid artery, was dissected and separated from the adjacent plaque (stable or noncomplicated plaque, NP), present in the common and external carotid arteries, as previously described.[19,20] Excised segments were immediately rinsed in ice-cold saline. Histological analysis of the samples showed that CPs corresponded to advanced type V or VI atherosclerotic lesions (mainly intraplaque hemorrhage evolving in the necrotic core) while the adjacent area (NP) was characterized as type III or IV lesions (lipid core encapsulated between a fibrous cap and the media)[21−23] according to the classification of Stary et al.[24]

Samples were rinsed in RPMI 1640, weighed, cut into 2−5 mm^3 pieces, and incubated in culture medium (RPMI 1640, 1% L-glutamine, 1% penicillin/streptomycin, and 1% amphotericin) at 37 °C (5% CO$_2$). The volume of culture medium was adjusted to tissue weight, at a ratio of 1:6 (mL/mg). After 24 h, the conditioned culture media containing the secreted plaque material were collected and rapidly cleared (4000 rpm, 1 min, 4 °C). Incubated tissue (CP and NP plaque material) and their corresponding conditioned media were kept separately at −80 °C until analysis.

2.4. Cell Culture. The T-lymphoma Jurkat cell line (gift from Pr. Robert Müller University of Mons-Hainaut, Belgium) was grown in RPMI-1640 medium supplemented with 10% fetal calf serum (FCS), 10 nM L-glutamine, and 5 μg/mL gentamycine. Human umbilical vein endothelial cells (HUVECs) (ATCC) were grown in EBM-2 medium supplemented with 5% FCS, 0.04% hydrocortisone, 0.1% ascorbic acid, 0.1% GA-1000, 0.1% heparin, and a mixture of growth factors (hFGF 0.4%, VEGF 0.1%, R^3-IGF 0.1%, and hEGF 0.1%).

Human THP-1 promonocyte cell line (ATCC) was grown in RPMI-1640 medium supplemented with 10% FCS, 10 nM L-glutamine, and a mixture of antibiotics (penicillin and streptomycin). The promonocytes were differentiated in macrophages by incubation with 200 nM PMA (phorbol myristate acetate) for 18 h at 37 °C in a humidified atmosphere and 5% CO$_2$. Differentiated macrophages are easily recognized by their shift from cells in suspension to adherent cells. Membrane expression of macrophage biomarker CD-14 was confirmed by flow cytometry. For this purpose, viable THP-1

macrophages were collected, counted, and resuspended in flow cytometry PBS (phosphate-buffered saline) supplemented with 0.1% BSA to a final concentration of 0.5×10^6 cells/mL. Subsequently, 2 μg of purified mouse FITC-conjugated monoclonal antihuman CD-14 antibody was incubated for 1 h at 4 °C while being sheltered from light. The cells were subsequently washed and suspended in flow cytometry buffer for analysis. Mouse nonspecific FITC-conjugated IgG was used as negative control.

Foam cell induction was obtained from PMA-differentiated macrophages which were washed three times with PBS and further incubated in RPMI (37 °C, 5% CO_2) supplemented with 100 μg/mL Ox-LDL (oxidized low-density lipoprotein) for 24 h. Immediately following incubation, culture medium was removed and cells were fixed in a 12-well dish, at a concentration of 10^6 cells/well, with 4% paraformaldehyde for 2−4 min. Lipid loading was verified by cell staining with 0.2% Oil-Red-O in methanol for 1−3 min. Cell count was performed using a light microscope (Leica DM IL HC) equipped with a 200× magnification lens. The cells were photographed using a Leica DC 300F Zoom Digital Camera. The number of foam cells formed was calculated and presented as percentage of foam cell formation. Flow cytometry measurements (FC500, Beckman Coulter, France) were also performed to evaluate the fraction of apoptotic and necrotic foam cells using a human annexin V-FITC (λ_{em} = 520 nm, FL1 reading)/propidium iodie (λ_{em} = 617 nm, FL3 reading) kit (Bender MedSystems, USA). To this end, cells were collected and resuspended in binding buffer (10 mM HEPES pH 7.4, NaCl 2.5 mM, $CaCl_2$ 1 mM), and their concentration was adjusted to 0.5×10^6 cells/mL. Subsequently, 5 μL of annexin V-FITC solution was incubated with 195 μL of the cell suspension for 10 min at room temperature (labeling of apoptotic cells). Cells were then washed and incubated with propidium iodide (1 μg/mL) to stain annexin-V responsive necrotic cells, which were finally detected by flow cytometry.

2.5. Ex Vivo Enzymatic Assay. A matrix metalloproteinase enzymatic activity assay was previously designed to quantify the MMP activity present in conditioned culture media obtained from atherosclerotic plaques of the internal carotid segments and of the common or external carotid segments, respectively.[16] Briefly, nonselective MMP substrate—7-methoxycoumarin-4-acetyl-Pro-Leu-Gly-Leu-β-(2−4-dinitrophenyl)-L-2.3-diamino-propionyl-Ala-Arg-NH_2 (Sigma, France) (20 μM)—and conditioned media (10 μL) from carotid tissues were incubated at 37 °C for 3 h in 50 mM Tris pH 7.5/10 mM $CaCl_2$/150 mM NaCl/0.05% Brij 35, supplemented with 30 nM retrothiorphan and 100 nM captopril to inhibit nonspecific cleavage by neprilysin and angiotensin-converting enzyme, respectively (final volume 100 μL). Released fluorescence, representing total activity, was measured at λ_{ex} = 340 nm and λ_{em} = 405 nm on a Twinkle LB970 apparatus (Berthold, Germany). Non-specific MMP activity (NSA) was measured under the same conditions except for the addition of the metal chelating agent EDTA (1 mM). Under these conditions, the specific MMP activity (SA) is equal to the total activity (TA) measured in the reaction buffer minus the NSA.

The enzymatic activities of NEP, ACE, ECE, APN, and APA were quantified in conditioned media using their respective specific fluorigenic assays. Enzymatic assays were performed using 10 μL of conditioned media in the reaction buffers described but supplemented with 0.05% Brij 35. The specific activity for each enzyme was evaluated by subtracting the

activity measured in the presence of 1 μM thiorphan for NEP, 1 μM captopril for ACE, 1 μM phosphoramidon for ECE, 1 μM RB3014 for APN, or 10 μM EC33 for APA.

Incubated tissue samples were weighed and homogenized in Tris 50 mM, Triton 0.1%, inhibitor cocktail without EDTA 0.1% (Sigma) in a weight to volume ratio of 50 mg of tissue for 1 mL of buffer. The enzymatic activities of MMPs and ACE were monitored as described above using 10 μL of tissue homogenate, while 5 μL was used to monitor that of APN. The ECE enzymatic activity was also searched using increasing quantities (10−30 μL) of tissue extract. Moreover, the enzymatic activities of these same proteases were also measured in the same fashion in THP-1 cell homogenates and conditioned culture medium.

2.6. Ex Vivo Inhibitory Potencies of P947 toward MMPs, APN and ACE in conditioned media from human atherosclerotic carotids. Ex vivo inhibitory potency (IC_{50}) of P947 toward MMPs in conditioned media was recently reported.[16] Briefly, the IC_{50} value of P947 for different MMPs expressed by the excised carotid tissues were evaluated by incubating equal quantities of conditioned media with increasing concentrations of P947 ranging from 10 nM to 1 μM in 100 μL assays. The value obtained in the presence of 1 mM EDTA, a non selective MMP inhibitor, was subtracted from each point to determine specific MMP activity. Inhibitory potencies of P947 toward ACE and APN expressed in these tissues were herein investigated in the same manner using their respective specific assay described in the above "ex vivo enzymatic assays" section. Taking advantage of their assay selectivity, measurement of IC_{50} values of P947 toward APN and ACE were translated into K_i values using the Cheng and Prussof equation (cf 2.2 section).

2.7. P947 binding to different cell types. THP-1 macrophages, THP-1 foam cells, T-lymphoma Jurkat cells or HUVECs were incubated (2×10^6 cells) with either P947 (active compound) or P1135 (inactive compound) at concentrations of 1 mM and 100 μM for 2 h, at 37 °C in a humidified atmosphere and 5% CO_2. The cells were then washed in PBS, centrifuged and the cell pellets collected and mineralized in nitric acid (80 °C, overnight) for quantification of cellular Gd uptake using Inductively Coupled Plasma-Mass Spectrometry (ICP-MS).

2.8. In vitro MRI of P947 or P1135-loaded THP-1 macrophages. A total of 10^7 THP-1 macrophages were incubated with 1 mM of either P947 or P1135 for 2 h at 37 °C. After washing and centrifugation, cell pellets were dispersed in 0.3 mL of 0.3% agar in a 48-well microplate at the concentration of 10^7 cells/well (300 μL). T1 mapping was assessed using an inversion−recovery rapid acquisition with relaxation enhancement (IR-RARE) sequence with eight inversion times (100−1700 ms). The parameters were TR = 3500 ms, effective TE = 40.8 ms, RARE factor =8, FOV = 8 × 5.5 cm, matrix =256 × 128, slice thickness =1.0 mm, interdistance =2.0 mm, flip angle =90°. A single IR-RARE image was obtained at the optimum inversion time (1.45 s) to provide a canceled agar signal. Signals were recorded using a 16-cm inner-diameter birdcage coil. At the end of the experiment, the cells were harvested, counted, and mineralized. Gd cellular uptake (fg Gd/cell) was measured by ICP-MS.

2.9. In vivo study (MRI and histology) of P947 in atherosclerotic rabbit model. *Animal model.* As previously described,[25] atherosclerotic plaques were induced in the abdominal aorta of 5 New Zealand White rabbits

(mean age 3 months; mean weight 2.7 ± 0.2 kg). A 4-month atherogenic diet was instituted, consisting of 0.3% cholesterol enriched food (SAFE 112). Two weeks after the start of the diet, animals were anesthetized with an intramuscular combination of ketamine and xylazine: a 4-French Fogarty embolectomy catheter was inserted into the right femoral artery and advanced in the aorta under fluoroscopy and withdrawn, with the balloon inflated, from descending thoracic aorta to the iliac bifurcation. Three weeks later, the same procedure was repeated through the left femoral artery. Five New Zealand White rabbits fed a chow diet were used as controls. All experiments were approved by the INSERM Animal Care and Use Committee.

In vivo MRI protocol.   Image acquisition. After four months of atherogenic diet, ten animals (five atherosclerotic rabbits and five controls) were imaged on a 1.5-T MRI system (Avanto; Siemens; Germany) Before each MR session, animals were anesthetized by intramuscular injection of an association of ketamine and xylazine and a cathether was placed in marginal ear vein. Animals were maintained on a supine position in the magnet. A small flex loop coil was positioned on the abdominal area. Care was taken in placing rabbits in identical positions in the coil for the different imaging. Ten sequential, 2-mm-thick, axial slices of the aorta were acquired from the celiac trunk to the iliac bifurcation using a fast spin−echo T1-weighted sequence giving an in-plane resolution of 400 × 400 μm (repetition time: 800 ms; echo time: 5.6 ms; field of view: 10 × 10 cm; matrix: 256 × 256; echo train length: 8; signal averages: 4; interslice gap: 3 mm). Inferior and superior radiofrequency saturation pulses were added to null the signal from flowing blood in the inferior vena cava and aorta, and spectral fat suppression to null the signal from the peri-adventitial fat.

A first MRI was performed before and 90 min after the intravenous injection of 50 μmol/kg of P947 in atherosclerotic ($n = 5$) and control ($n = 5$) rabbits. The same rabbits were imaged a week later before and 90 min after injection of Dotarem (Guerbet, Aulnay-Sous-Bois, France).

Image analysis. MR images were analyzed with ImagePro Plus (Media Cybernetics). Signal intensities were measured in each rabbit on 10 sequential axial T1-weighted images before and 90 min after injection of each contrast agent. Origin of the left renal artery and iliac bifurcation were identified on each MRI acquisition and used to ensure identical slice positions between pre- and postcontrast images and between the different MRIsperformed on the same rabbit. Regions of interest (ROI) encompassing the aortic wall were drawn manually on the MR acquisition obtained 90 min after injection of the contrast agent. These ROIs were then copied on each axial slice of the acquisitions obtained before the injection of contrast agent. Areas and mean signal intensities (SI) of the aortic wall were then measured in these ROIs by an operator blinded to rabbit group and injected contrast agent. Standard deviation (SD) of noise was measured in a ROI located outside the rabbit. The aortic wall enhancement (%) was calculated using the following formula:

$$\text{Aortic wall enhancement}$$
$$= ((\text{SNR postcontrast} - \text{SNR precontrast})$$
$$/\text{SNR precontrast}) \times 100$$

where Signal to Noise Ratio (SNR) of aortic wall was defined as the SI of aortic wall/SD of noise.

2.10. Statistical analysis. Cellular Gd concentrations and $T1$ values, were compared using paired Student t test. The MMP activities of unstable and stable plaques from carotid artery were also compared with a paired Student t test. Differences were considered significant at $P < 0.05$. Comparison of the two groups of rabbits were performed using a one-way ANOVA test and posthoc Bonferroni t test.

3. RESULTS

3.1. *In vitro* inhibitory potency of P947 toward MMPs, ACE, APA, APN, ECE-1 and NEP. We recently reported that P947 inhibited the activities of a broad spectrum of recombinant purified MMPs with affinities in the micromolar range.[16] In the present work, we further investigated the inhibitory potencies (K_i) of this same compound toward related zinc-dependent metalloproteinases, e.g. ACE, APA, APN, ECE and NEP. The ability of P947 to bind, and thus inhibit, the catalytic site the various metalloproteinases was evaluated *in vitro* by measuring the inhibition of enzyme activities. Table 1

Table 1. *In vitro* affinities of P947 against various metalloproteinases: specific fluorigenic assays were performed as described in experimental procedure. The Ki values for P947 were calculated using the Cheng-Prusoff equation ($Ki = IC_{50}/[1+(S/K_m)]$) based on data analyzed using Graph Pad PRISM® software v4.0

Metalloproteinase	K_i (μM)
MMP-2	2.75 ± 0.03
ACE	24.00 ± 0.04
APA	24.10 ± 0.06
APN	16.10 ± 0.02
ECE-1	7.30 ± 0.02
NEP	23.70 ± 0.03

reports the K_i values of P947 toward each of these enzymes. We previously demonstrated that the affinities of P947 toward various MMP subtypes ranged between 0.1 μM (MMP-8) and more than 10 μM (MMP-3) reflecting the broad spectrum profile of the compound for the MMP family.[16] The inhibitory potencies of P947 toward the APN and APA aminopeptidases were of 16.10 ± 0.02 and 24.10 ± 0.06 μM, respectively. P947 also inhibited NEP (K_i = 23.70 ± 0.03 μM) and ACE (K_i = 24.00 ± 0.04 μM) with similar affinities, while it inhibited ECE-1 activity with the highest potency, i.e. 7.30 ± 0.02 μM. Although these potencies are several orders of magnitude lower than those of their respective specific inhibitors, the values are nevertheless in the same range as those measured for various MMPs. The scrambled product P1135 revealed no affinity for any of the tested metalloproteinase, thus confirming its adequacy as a reference compound.

3.2. MMPs, APN, APA, NEP, ACE, and ECE-1 Activities in Stable and Culprit Plaques from Atherosclerotic Human Carotids. Specific enzymatic assays were used to quantify the activities of the above-defined *in vitro* targets of P947, i.e. metalloproteinases which recognized and bound the contrast agent with micromolar potencies. Thus, conditioned media obtained from human atherosclerotic carotid samples were shown to contain specific MMP activity as well as specific enzymatic activities corresponding to ACE and APN expression (see below). Interestingly, the specific enzymatic activities of APA, NEP, and ECE were found to be negligible. Because of possible discrepancies in the subcellular distributions of these

Conditioned Media   Tissue Homogenate
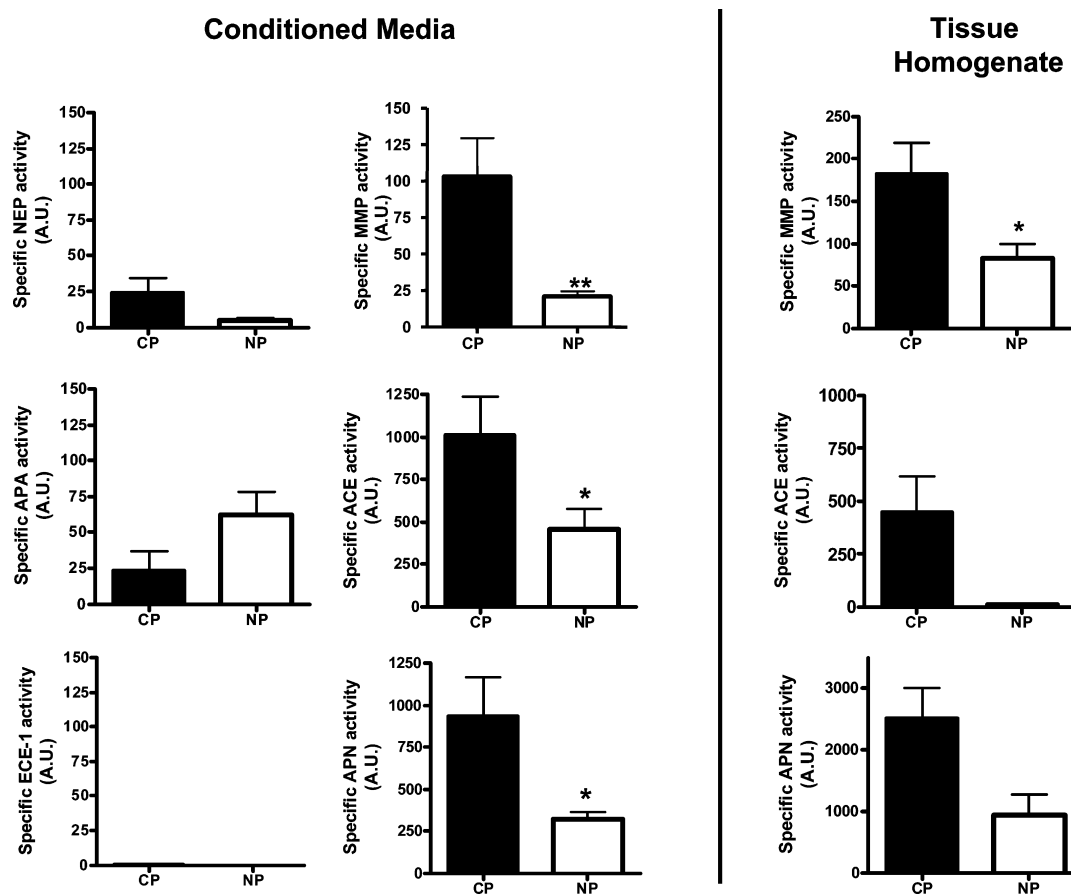
Figure 1. MMPs, APN, APA, NEP, ACE, and ECE activities in culprit (CP) and stable, noncomplicated (NP) atherosclerotic plaques from human carotids. The expression of various metalloproteinases in conditioned media (10 μL) form culprit and stable zones of human plaque samples collected from patients undergoing carotid endarterectomy was investigated using specific fluorigenic assays. Using conditioned media produced from samples collected from two patients, NEP, APA, and ECE-1 activities were found to be negligible whereas MMP, ACE, and APN activities were systematically and reproducibly measured. Expression of MMP was significantly more abundant in culprit (CP) than in the adjacent stable (NP) zone ($n = 12$, $P < 0.005$), as was that of ACE ($n = 7$, $P < 0.05$) and APN ($n = 7$, $P < 0.05$). These results were confirmed using the corresponding incubated tissue homogenates, which are shown to express MMP, ACE, and APN enzymatic activities with the same tendency as that observed in conditioned media. A.U.: arbitrary unit. * P < 0.05; **P < 0.005.

latter metalloproteinases, which are known to be membrane bound ecto-proteases but which can also be found as secreted forms in the plasma, tissues used to produce the conditioned media were homogenized and the enzymatic activities therein measured in the same fashion. Results of these experiments paralleled the results observed in the conditioned media, showing weak or the absence of expression of APA, NEP and ECE in tissue homogenates (data not shown).

Conditioned media of stable and culprit plaques from several patients were used to search for differences in the expression of the newly defined P947 targets. Results showed a significant ($n = 12$, $P = 0.0046$), 5-fold increase in MMP activity in culprit versus stable plaques (Figure 1). Moreover, there was also significantly more ACE ($n = 7$, $P = 0.015$) and APN ($n = 7$, $P = 0.04$) activities detected in vulnerable versus stable plaques from the same patients, each being increased ~2- and ~3-fold, respectively. The enzymatic activities of MMPs, APN, and ACE measured in tissue homogenates also showed similar tendencies, as homogenates from the vulnerable, CP lesions were found to contain ~2, ~2.3, and several hundred-fold more MMP, APN, and ACE activities, respectively, as compared to homogenates from stable NP plaques.

3.3. *Ex Vivo* Potencies of P947 toward MMPs, ACE, and APN in Stable and Culprit Plaques from Human Atherosclerotic Carotid Samples.

In a recent study, we showed that P947 was dose-dependently able to inhibit MMP activities from conditioned media of three culprit and three stable plaques.[16] Mean IC_{50} values were measured at 8.6 ± 3.0 μM and 7.5 ± 2.8 μM, respectively (Figure 2A). In the present study, five out of the seven conditioned media samples used for ACE and APN quantification were also used to determine the *ex vivo* affinity of P947 toward these metalloproteinases. For ACE, the K_i values of P947 ranged between 4 and 10 μM, for culprit plaques (CP), and they ranged between 4 and 15 μM for stable (NP) plaque (Figure 2B). The resulting mean K_i values of 6.4 ± 2.7 μM and 9.1 ± 3.8 μM, for culprit and stable plaques, respectively, were not statistically different, suggesting that the conformation of the protein is unaltered. Study of the affinity of P947 toward APN revealed similar results inasmuch as the mean K_i values obtained using conditioned media from either stable or vulnerable plaques were not statistically different (3.3 ± 0.88 μM and 2.1 ± 0.4 μM, respectively) (Figure 2C).

3.4. Validation of Macrophage and Foam Cell Models.
The phagocytic phenotype of PMA-differentiated THP-1 was
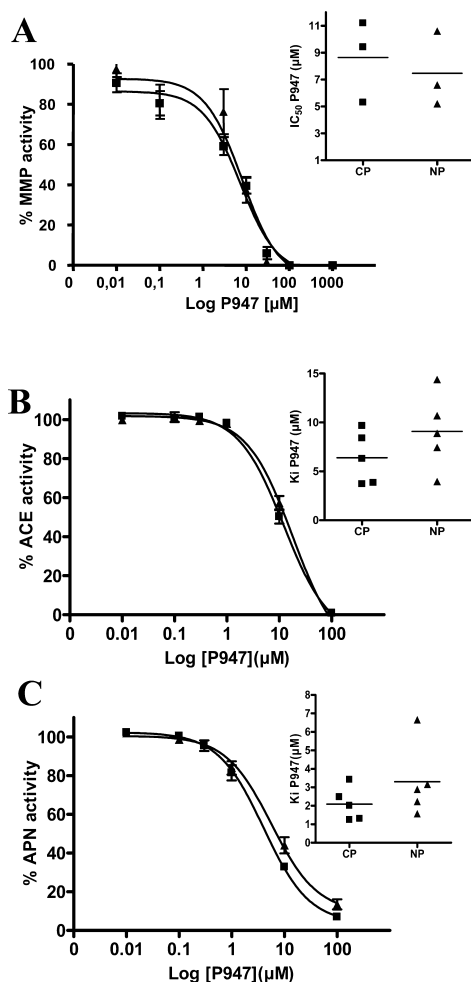
Figure 2. *Ex vivo* inhibitory potency of P947 toward MMPs, APN, and ACE in conditioned media from human atherosclerotic carotids: Increasing concentrations of P947 were placed in the presence of conditioned media from culprit plaques (CP, ■) or noncomplicated (NP) plaques (▼). Represented in part A are the previously obtained mean IC$_{50}$ curves of P947 against MMPs expressed in conditioned media.[16] Individual IC$_{50}$ values are represented in the associated scatter plot. The data plotted in part B are mean inhibitory values of P947 against ACE obtained from five tested samples in duplicate. The calculated individual K_i values are shown in the accompanying scatter plot. Part C shows the data obtained for APN.

confirmed using flow cytometry and revealed intense expression of the CD-14 macrophage marker at the cell surface, with 100% of labeled cells and about a 35-fold increase

of immunostaining with specific anti-CD-14 as compared to the control isotype (see the Supporting Information).

MMPs, ACE, and APN enzymatic activities expressed in THP-1 macrophage homogenates and in their conditioned culture medium were quantified using specific fluorigenic assays. While MMPs activity was measured both in macrophagic cell homogenates and in culture medium, APN activity was mainly detected in the cell fraction and ACE activity was predominantly found in the culture medium. This suggests that ACE is shed from these cells (Figure 3). Taken together, these data suggest that THP-1 macrophages represent an appropriate model for the study of P947 binding to these enzymes, especially MMP and APN, which were highly expressed by the cell homogenates and, thus, likely at their surface.

O-Red-Oil staining allowed for discrimination between Ox-LDL-treated (foam cells, Figure 4B) and nontreated (Figure 4A) THP-1 macrophages and showed that about 80% of macrophages stained positively. As expected, the foam cell phenotype led to an increase of the apoptotic/necrotic index in these cells. This was confirmed by flow cytometry measurement of double annexin V-FITC/propidium iodide labeled cells, which showed an increase in the percentage of double labeled cells, i.e. from 14.6% of apoptotic/necrotic cells for monocytes THP-1 (Figure 4C) to 28.7% for Ox-LDL-treated foam cells (Figure 4D).

3.5. P947 Labeling of THP-1 Macrophages, THP-1 Foam Cells, HUVEC, and T-Lymphocyte Jurkat Cell Lines. Different P947 labeling patterns were observed according to cell types (Table 2).

In HUVEC cells, Gd cellular accumulation was not significantly different between P947 and P1135 (61.4 ± 23.9 fg Gd/cell vs 40.2 ± 6.9 fg Gd/cell at the highest incubation concentration). Nevertheless, the grafting of either active (P947) or inactive (P1135) peptide to Gd-DOTA led to a stronger binding by HUVECs as compared to the reference compound Gd-DOTA (21.5 ± 2.6 fg Gd/cell at 1 mM incubation). The same labeling pattern was observed at a lower concentration (0.1 mM), but with a smaller magnitude.

In Jurkat T lymphocytes, P947 labeling was not different from that of the reference product Gd-DOTA, at both 1 mM and 0.1 mM (Table 1).

The signal measured on THP-1 macrophages labeled with either active or control compounds was concentration-dependent (Table 2). Grafting of active peptide potentiated P947 binding to macrophages from 2.3 ± 1.0 fg Gd/cell (at 0.1 mM Gd incubation) to 14.6 ± 4.5 fg Gd/cell (1 mM Gd incubation). The signal returned to the background level (identical to Gd-DOTA) when using the P1135 scrambled product: 0.5 ± 0.2 fg Gd/cell (0.1 mM incubated) and 6.2 ± 1.5 fg Gd/cell
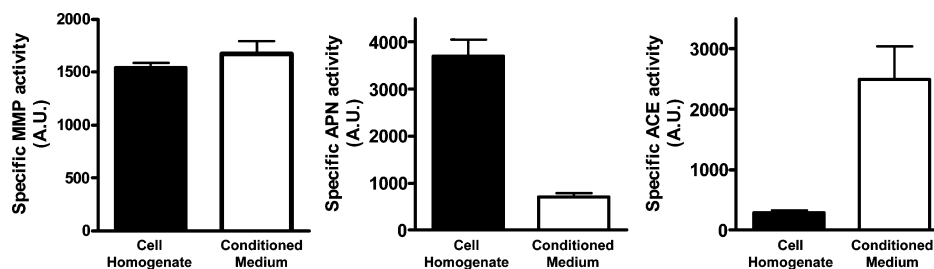
Figure 3. MMPs, APN, and ACE activities in the THP-1 macrophage model. Macrophage cell homogenates (4.38 × 10^5 cells) and conditioned culture media (30 μL) were assayed for their content in MMPs, ACE, and APN enzymatic activity. Whereas active MMPs were found in both cells and culture media, ACE was mainly expressed in the culture medium, while APN was essentially measured using the cell homogenate. A.U.: arbitrary unit.
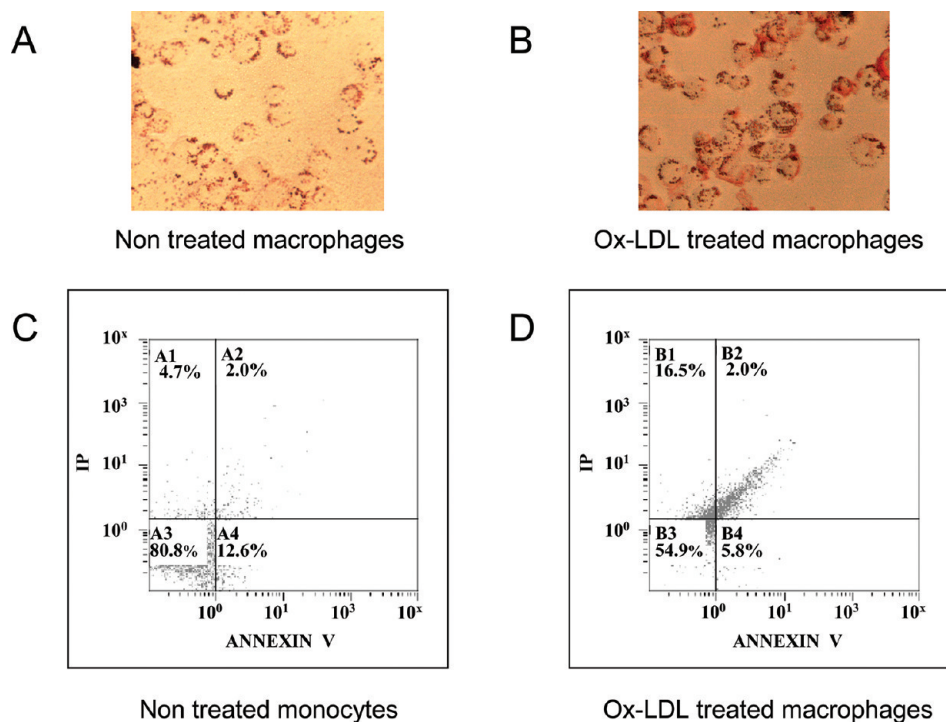
Figure 4. Characterization of Ox-LDL treated THP-1 foam cells. The induction of foam cells was obtained from PMA-differentiated macrophages which were incubated with (B) or without (A) 100 μg/mL Ox-LDL for 24 h. Lipid loading was verified by staining with 0.2% Oil-Red-O in methanol for 1−3 min. Cells were observed and counted using a light microscope (Leica DM IL HC) with 200× magnification. Flow cytometry measurements were performed to detect apoptotic and necrotic foam cells using a human annexin V-FITC (λ_{em} = 520 nm, FL1)/propidium iodie kit (λ_{em} = 617 nm, FL3).

Table 2. Gd Accumulation in Various Cell Models[a]

	P947		P1135		Dotarem	
	1 mM	0.1 mM	1 mM	0.1 mM	1 mM	0.1 mM
THP-1 macrophages	14.6 ± 4.5[b,c]	2.3 ± 1.0[b,c]	6.2 ± 1.5	0.5 ± 0.2	6.1 ± 0.9	0.5 ± 0.1
THP-1 foam cells	7.2 ± 0.3[b]	1.3 ± 0.2[b]	4.6 ± 0.6	0.3 ± 0.1	n.d.	n.d.
HUVEC	61.2 ± 23.9[c]	10.5 ± 2.6[c]	40.2 ± 6.9[c]	8.2 ± 21.9[c]	21.5 ± 2.6	2.2 ± 0.5
T-lymphocyte Jurkat	53.4 ± 23.5	5.6 ± 2.8	n.d.	n.d.	49.7 ± 17.8	5.4 ± 2.5

[a]Results are expressed in fg Gd/cell measured after 2 h incubation (37 °C) of either P947, P1135, or Dotarem with THP-1 macrophages, THP-1 foam cells, HUVEC, or the T-lymphocyte Jurkat cell line. n.d. stands for not determined. [b]$P < 0.05$ (Student's t test) as compared to P1135 at the same concentration. [c]$P < 0.05$ (Student's t test) as compared to Dotarem at the same concentration.

(1 mM incubated). These data showed a significantly different labeling intensity with active P947 as compared to either inactive scrambled P1135 or reference Gd-DOTA products. As the comparison with P1135 allowed the demonstration of a specific labeling of P947 by macrophages, the reference product Gd-DOTA was not tested in the foam cell model and P1135 was used as the only control product. Similarly to THP-1 macrophages, the labeling intensity of foam cells by active P947 was significantly higher than that measured with the scrambled P1135 product at an either 1.0 or 0.1 mM concentration.

3.6. Specific Metalloproteinase-Targeting of P947 and Detection by MRI in THP-1 Macrophages. Metalloproteinase-targeting of P947 in THP-1 macrophages was investigated by a fluorigenic approach using specific substrates. Thus, the MMPs activity in THP-1 macrophages inhibited by 1 mM P947 (70%) or 1 μM NNGH (35%) another broad spectrum, low affinity inhibitor of MMP activity (Figure 5A). Similarly, the macrophagic APN activity was almost completely inhibited (95%, Figure 5) by either 1 mM P947 or 1 μM RB-3014 (specific, high affinity APN-inhibitor). Taken together, these

data confirm an MMP- and APN-binding potency of P947 in the THP-1 macrophage model.

After incubating THP-1 macrophages with 1 mM either P1135 or P947 for 2 h, $T1$ values, measured from MR images, decreased from 2.094 ± 0.007 s (THP-1 alone) to 2.049 ± 0.005 s (P1135), and finally to 2.004 ± 0.014 (P947) s (Figure 5B). This decrease produced a higher enhancement of the MRI signal with P947 than with P1135 (Figure 5B). Changes in $T1$ detected with P947 were confirmed by measurements of Gd cellular concentration values measured by ICP-MS—undetectable for THP-1 alone, 5.18 ± 0.43 fg Gd/cell for P1135 and 11.01 ± 1.05 fg Gd/cell for P947, i.e. 5.83 fg Gd/cell (P947−P1135)—and were correlated with the metalloproteinase activities of MMPs and APN measured in THP-1 macrophages.

3.7. In Vivo Study of P947 in the Atherosclerotic Rabbit Model. The intensity of the aortic wall enhancement (Figure 6) was significantly ($P < 0.05$) higher 90 min after injection of P947 than after injection of Dotarem in atherosclerotic rabbits (respectively 44 ± 11% and 11 ± 4%; $P < 0.05$). In contrast, the aortic wall enhancement was similar

Group	THP-1 alone	P947 (1 mM)	P1135 (1 mM)
MR images			
$T1$ value (sec)	2.094 ± 0.007	2.004 ± 0.014	2.049 ± 0.005
Gd amount (fg Gd/cell)	n.s.	11.01 ± 1.05	5.18 ± 0.43
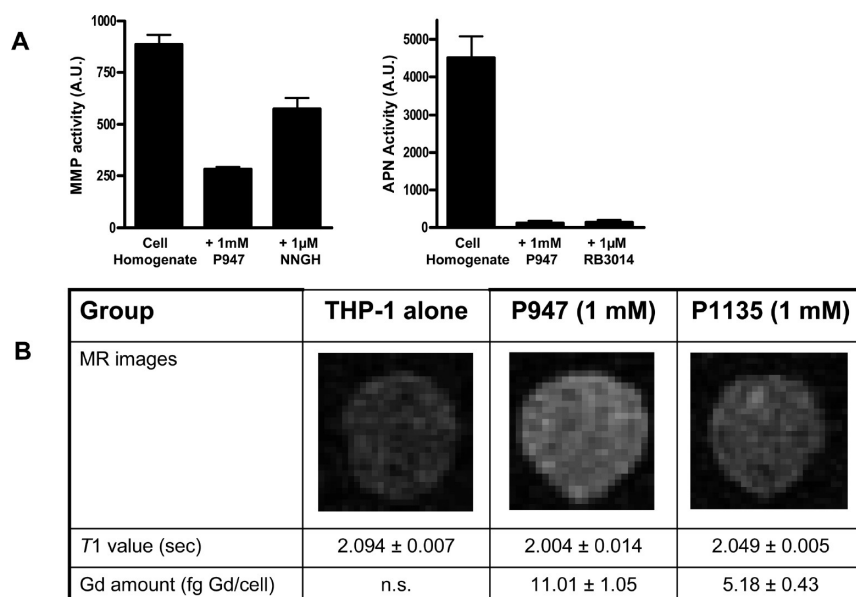
Figure 5. Detection of metalloproteinase binding of of P947 by fluorimetric assay and MRI procedure. (A) The binding capacity of P947 (1 mM) toward MMPs and APN expressed in macrophage cell homogentaes (4.38×10^5 cells) was evaluated in vitro using enzymatic fluorigenic assays for each enzyme. P947 inhibited 70% of the cellular MMP activity, while the broad spectrum NNGH inhibitor inhibited about 35% of the same activity. APN activity was fully (~95%) inhibited by P947 and its specific, high affinity inhibitory RB3014 compound. (B) Macrophages were incubated with 1 mM of either P947 or P1135 for 2 h at 37 °C. Cell pellets were dispersed in 0.3 mL of 0.3% agar in a 48-well microplate at a concentration of 10^7 cells/well (300 μL). $T1$ mapping was assessed using an inversion−recovery rapid acquisition with a relaxation enhancement (IR-RARE) sequence with eight inversion times (100−1700 ms). The parameters were TR = 3500 ms, effective TE = 40.8 ms, RARE factor = 8, FOV = 8×5.5 cm, Mx = 256×128, Sl. Th = 1.0 mm, Interdist. = 2.0, F.A. = 90°. At the end of the experiment, the Gd cellular uptake was measured by ICP-MS. A.U.: arbitrary unit.
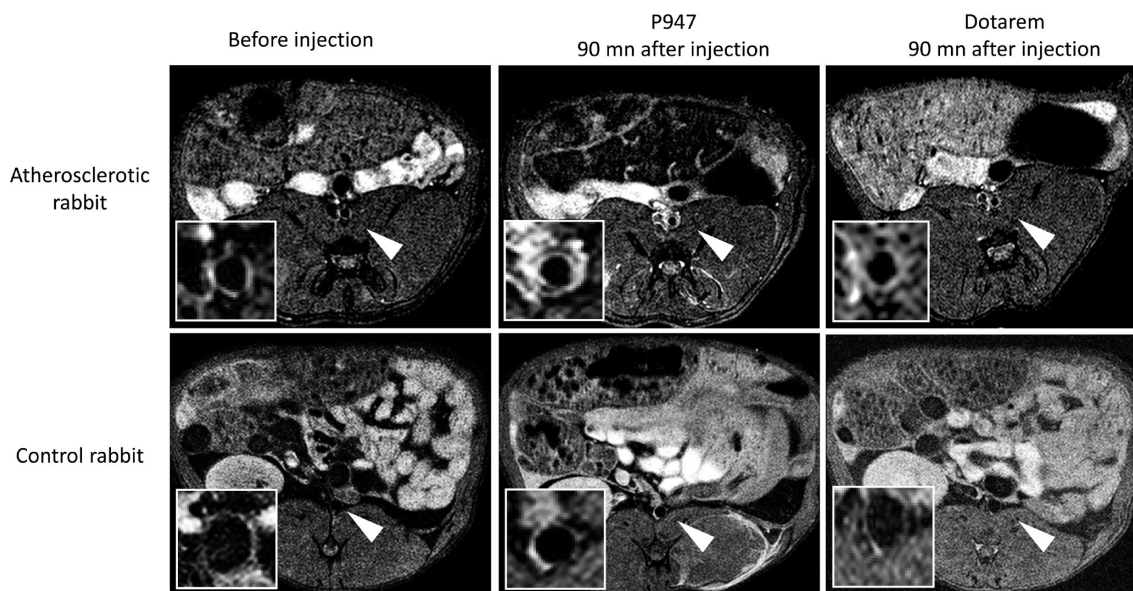
Figure 6. Axial T1-weighted images performed on the middle part of the aortic wall, before and 90 min after injection of 50 μmol Gd/kg P947 or 50 μmol Gd/kg Dotarem in atherosclerotic rabbit (upper images) or control rabbit (lower images). Note that enhancement of the aortic wall was more intense after injection of P947 than after injection of Dotarem in atherosclerotic rabbit. No significant enhancement was detected in control rabbit after injection of P947 or Dotarem.

90 min after injection of P947 and Dotarem in control rabbits ($9 \pm 3\%$ and $3 \pm 4\%$, respectively; P = NS).

4. DISCUSSION AND CONCLUSIONS

This study aimed to identify and describe the molecular and cellular action mechanisms of the newly designed contrast agent P947, a potential tool for the detection and characterization of the MMP-rich atherosclerotic plaques by MRI.[16]

First, this study confirmed previous studies that reported an up-regulation of most MMPs[26−35] (MMP-1, -2, -3, -7, -8, -9, -11, -12, -13, -14, and -16), especially in macrophages, which are known to be involved in the vulnerability of these lesions. In this study, we confirmed increased enzymatic activity of MMPs using an alternate, more rapid, and direct fluorigenic method. The MMP family is constituted of a large number of metalloproteinases. Although all cleave components of the

ECM have similar structure, directed to the constitutive pathway, they differ in their subcellular distributions: the majority are soluble secreted enzymes, while others are found on the plasmic membrane, in contact with the extracellular space (e.g., MMP-14 and -16). Enzymatic assays confirmed ACE[36−40] expression in human atherosclerotic plaques but also demonstrated a physiologically relevant increased APN enzymatic activity. Indeed, using atherosclerotic culprit CP plaque tissue and adjacent NP tissue samples from human carotid endarterectomy and their conditioned culture media, we have shown that MMPs and ACE activities are increased several-fold in culprit plaques (CP) as compared to stable (NP) plaques. These higher enzymatic activities were observed both in tissue homogenates and conditioned media, suggesting that expression of both cellular and secreted active enzyme forms are up-regulated in culprit plaques (Figure 1). Moreover, their unaltered affinities toward the P947 in both culprit and stable plaques strongly argue against any structural modifications of these enzymes. To our knowledge, this is the first time that an increased APN expression and activity have been detected in culprit human atherosclerotic plaques. Aminopeptidase N, also referred to as alanine aminopeptidase, is a ubiquitous ectoenzyme involved in the inactivation of bioactive peptides such as the enkephalins.[41] Its role in the development of atherosclerotic plaque, especially in the process of instability, however, remains to be explored. The potential involvement of this type of metalloproteinase in arterial hypertension and cardiovascular diseases was recently evidenced by a genetic study linking a newly identified polymorphism within the coding sequence of a related aminopeptidase with blood pressure.[42] ECE-1 is a zinc dependent metalloproteinase of the constitutive pathway responsible for the production of biologically active endothelin, a highly vasoconstrictive peptide. The lack of ECE-1 activity in carotid atherosclerotic plaques, both culprit and stable, is not consistent with the reported enhancement of ECE-1 expression and activity in coronary atherosclerotic plaques.[43−45] Although this difference could lie in the different methods used to detect ECE-1 enzymatic activity, it may also be that ECE-1 is differently and specifically regulated according to the vascular territories.

In the present study, the previously established MMP-targeted profile of P947 was completed by the demonstration of a wider affinity pattern including other types of metalloproteinases.[16] Indeed, the *in vitro* inhibitory potencies of P947 toward recombinant or native purified ACE, APN, APA, ECE-1, and NEP were similar to its potency toward MMPs (micromolar affinities, Table 1). This is most likely attributable to the grafting of an inhibitory peptide containing a hydroxamate zinc-chelating moiety at its extremity onto Gd-DOTA. Thus, the broader inhibitory spectrum of P947, providing the contrast agent with a greater binding capacity, should allow for accumulation of higher amounts of the MRI contrast agent in metalloproteinase-activated tissues, i.e. tissues accumulating increased enzymatically active proteases at their surface and/or increased content in the metalloproteinase expressing macrophagic cells. As P947 is shown here to bind MMPs, ACE, and APN enzymes in atherosclerotic plaques with the same potency (similar affinities), this MRI contrast agent could represent an appropriate tool for detecting the activity of metalloproteinases in pathological tissues. Thus, differences in MRI signal should reflect the quantity of active metalloproteinase activities *in situ*. In atherosclerotic patients, this

information could help to characterize atherosclerotic plaques and their risk of rupture.

The high binding of targeted P947, but also of nontargeted P1135 and nonspecific MRI product Gd-DOTA, by endothelial and lymphocyte cells suggests a nonspecific accumulation of Gd chelates within these cells (Table 2). This could explain the previously reported heterogeneity of the enhanced MRI pattern after injection of P947 in apoE$^{-/-}$ mice[17] (atherosclerotic plaque model), with a variable background of P947 accumulation in vascular territories in which endothelial and lymphocyte cells are present.

On the other hand, the specific binding of P947 to THP-1 macrophages is of particular interest because macrophages represent the main inflammatory cell type involved in initiation, progression, and aggravation processes which finally culminate in plaque rupture and possibly vessel thrombosis.[3] In our study, we showed that MMPs, ACE, and APN activities identified in culprit atherosclerotic plaques are also expressed in the THP-1 macrophage cell model. Indeed, MMPs activity was found in the macrophagic cells, both as cell-bound and secreted forms. APN activity was mainly detected in the cell homogenates while ACE activity was predominantly found in the conditioned culture medium, suggesting that this latter metalloproteinase is secreted and, thus, may not participate in the labeling of these cells by P947 (Table 2, Figure 3). These data confirm that THP-1 macrophages are an appropriate model to study the binding of P947 through a complex metalloproteinase pathway. As expected, the grafting of an active broad spectrum metalloproteinase-inhibitory peptide onto a Gd chelate, as called P947, yielded a high macrophagiclabeling, as compared to the nontargeted P1135 (grafted with a scrambled peptide) or to the nonspecific compound Gd-DOTA. Results of the specific MMP and APN enzymatic assays strongly suggest that this accumulation is mediated by MMP- and APN-targeting mechanisms. Interestingly, specific labeling was detected by MRI in an *in vitro* assay showing a higher MR signal for P947 than for P1135 or for cells incubated without any product (Figure 5). This result suggests that P947 was accumulated at the surface of macrophages, through MMP and APN binding, reaching MRI sensitivity threshold levels. This result moreover confirms those previously observed *in vivo* in the aorta of apoE$^{-/-}$ mice[16] or those of the present study in the atherosclerotic rabbit model, which can be considered as a more predictive model for future clinical imaging. Moreover, the amount of P947 measured in foam cells (Ox-LDL-treated THP-1) was significantly higher than that of the scrambled product P1135, suggesting that the specific MRI signal detected in both atherosclerotic mouse and rabbit models could also be explained by an effective foam cell labeling. Lastly, our *in vivo* MRI measurements in atherosclerotic rabbits confirmed the capacity of P947 to detect differences in the MR enhancement of the aortic wall between normal and atherosclerotic rabbits which had been previously demonstrated by Hyafil et al.[46]

In summary, we show in this study that P947, a new MR contrast agent, designed for plaque imaging, targets MMPs activity but also ACE and APN activities. The originality of P947 lies in its broad spectrum metalloproteinase inhibitor targeting moiety, which appears optimal for molecular MRI. The efficiency of the nonselective metalloproteinase targeting has already been demonstrated in previous studies. For example, the nonselective MMP inhibitors, batimastat and marimastat, were shown to efficiently prevent restenosis after balloon dilatation in atherosclerotic pigs.[47] Moreover, scintigraphic imaging has also

demonstrated the "broad spectrum" proof-of-concept in imaging with the nonselective MMP inhibitor [123I]-CGS 27023A,[48] which allowed the in vivo detection of MMP-rich vascular lesions in ApoE$^{-/-}$ mice. As demonstrated by our study, numerous active forms of metalloproteinases are involved in the development of the atherosclerotic plaque rather than a specific one. The potential added strength of targeting an even wider variety of enzymes with a targeted MRI contrast agent such as P947 is (1) to reach enough sensitivity to detect activated enzymes by MRI and (2) to detect a biological mechanism in its integrity and complexity, such as a physiological and local integrator of the progression of the plaque. First, preclinical toxicological investigations in mice or in vitro models (DL$_{50}$, CEL$_{50}$, hemodynamics, and complement system studies) with P947 are in favor of its safety. Molecular imaging using this new targeted MRI agent could provide promising tools to identify the vulnerability of atherosclerotic plaques in humans and improve our understanding of the role of metalloproteinases in plaque progression.

■ ASSOCIATED CONTENT

ⓢ Supporting Information

Flow cytometry measurements. This material is available free of charge via the Internet at http://pubs.acs.org.

■ AUTHOR INFORMATION

Corresponding Author

*Guerbet, Research Center, 16-24 rue Jean Chaptal, 93600 Aulnay-sous-Bois, France. Telephone/Fax: +33-1.45.91.69.64/ 51.23. E-mail: Sebastien.Ballet@guerbet-group.com.

Notes

The authors declare the following competing financial interest(s):Some authors are Guerbet employees in the Research Department, which is the inventor of the P947 product.

■ REFERENCES

(1) Pasterkamp, G.; de Kleijn, D. P.; Borst, C. Arterial remodelling in atherosclerosis, restenosis and after alteration of blood flow: potential mechanisms and clinical implications. *Cardiovasc. Res.* **2000**, *45*, 843–852.

(2) Ward, M. R.; Pasterkamp, G.; Yeung, A. C.; Borst, C. Arterial remodeling. Mechanisms and clinical implications. *Circulation* **2000**, *102*, 1186–1191.

(3) Hansson, G. K. Inflammation, atherosclerosis, and coronary artery disease. *N. Engl. J. Med.* **2005**, *352*, 1685–1695.

(4) Shimada, K. Immune system and atherosclerotic disease: heterogeneity of leukocyte subsets participating in the pathogenesis of atherosclerosis. *Circ. J.* **2009**, *73*, 994–1001.

(5) Nagase, H.; Visse, R.; Murphy, G. Structure and function of matrix metalloproteinases and TIMPs. *Cardiovasc. Res.* **2006**, *69*, 562–573.

(6) Dollery, C. M.; Libby, P. Atherosclerosis and proteinase activation. *Cardiovasc. Res.* **2006**, *69*, 625–635.

(7) Newby, A. C. Metalloproteinase expression in monocytes and macrophages and its relationship to atherosclerotic plaque instability. *Arterioscler., Thromb., Vasc. Biol.* **2008**, *25*, 2108–2114.

(8) Daugherty, A.; Manning, W.; Cassis, L. A. Angiotensin II promotes atherosclerotic lesions and aneurysms in apolipoprotein E-deficient mice. *J. Clin. Invest.* **2000**, *105*, 1605–1612.

(9) Keidar, S.; Kaplan, M.; Aviram, M. Angiotensin II-modified LDL is taken up by macrophages via the scavenger receptor leading to cellular cholesterol accumulation. *Arterioscler. Thromb. Vasc. Biol.* **1996**, *16*, 122–129.

(10) Keidar, S.; Attias, J.; Heinrich, R.; Coleman, R.; Aviram, M. Angiotensin II atherogenicity in apolipoprotein-E-deficient mice is associated with increased cellular cholesterol biosynthesis. *Atherosclerosis* **1999**, *146*, 246–257.

(11) Keidar, S.; Heinrich, R.; Kaplan, M.; Hayek, T.; Aviram, M. Angiotensin II administration to atherosclerotic mice increases macrophage uptake of Ox-LDL: a possible role for interleukin-6. *Arterioscler., Thromb., Vasc. Biol.* **2001**, *21*, 1464–1469.

(12) Diet, F.; Pratt, R. E.; Berry, G. J.; Momose, N.; Gibbons, G. H.; Dzau, V. J. Increased accumulation of tissue ACE in human atherosclerotic coronary artery disease. *Circulation* **1996**, *94*, 2756–2767.

(13) Fukuhara, M.; Geary, R. L.; Di,z, D. I.; Gallagher, P. E.; Wilson, J. A.; Glazier, S. S.; Dean, R. H.; Ferrario, C. M. Angiotensin-converting enzyme expression in human carotid artery atherosclerosis. *Hypertension* **2000**, *35*, 353–359.

(14) Ribichini, F.; Pugno, F.; Ferrero, V.; Bussolati, G.; Feola, M.; Russo, P.; Di Mario, C.; Colombo, A.; Vassanelli, C. Cellular immunostaining of angiotensin-converting enzyme in human coronary atherosclerotic plaques. *J. Am. Coll. Cardiol.* **2006**, *47*, 1143–1149.

(15) Schieffer, B.; Schieffer, E.; Hilfiker-Kleiner, D.; Hilfiker, A.; Kovanen, P. T.; Kaartinen, M.; Nussberger, J.; Harringer, W.; Drexler, H. Expression of angiotensin II and interleukin 6 in human coronary atherosclerotic plaques: potential implications for inflammation and plaque instability. *Circulation* **2000**, *101*, 1372–1378.

(16) Lancelot, E.; Amirbekian, V.; Brigger, I.; Raynaud, J. S.; Ballet, S.; David, C.; Rousseaux, O.; Le Greneur, S.; Port, M.; Lijnen, H. R.; Bruneval, P.; Michel, J. B.; Ouimet, T.; Roques, B.; Amirbekian, S.; Hyafil, F.; Vucic, E.; Aguinaldo, J. G.; Corot, C.; Fayad, Z. A. Evaluation of matrix metalloproteinases in atherosclerosis using a novel noninvasive imaging approach. *Arterioscler., Thromb., Vasc. Biol.* **2008**, *28*, 425–432.

(17) Aubry, M.; Berthelot, A.; Beaumont, A.; Roques, B. P.; Crine, P. The use of a monoclonal antibody for the rapid purification of kidney neutral endopeptidase ("enkephalinase") solubilized in octyl glucoside. *Biochem. Cell. Biol.* **1987**, *65*, 398–404.

(18) Piquilloud, Y.; Reinharz, A.; Roth, M. Studies on the angiotensin converting enzyme with different substrates. *Biochim. Biophys. Acta* **1970**, *206*, 136–142.

(19) Ouimet, T.; Orng, S. V.; Poras, H.; Gagnidze, K.; Devi, L. A.; Fournié-Zaluski, M. C.; Roques, B. P. Identification of an endothelin-converting enzyme-2-specific fluorigenic substrate and development of an in vitro and ex vivo enzymatic assay. *J. Biol. Chem.* **2010**, *285*, 34390–34400.

(20) Poras, H.; Ouimet, T.; Orng, S. V.; Dangé, E.; Fournié-Zaluski, M. C.; Roques, B. P. Pluripotentialities of a quenched fluorescent peptide substrate library: enzymatic detection, characterization, and isoenzymes differentiation. *Anal. Biochem.* **2011**, *419*, 95–105.

(21) Leclerq, A.; Houard, X.; Philippe, M.; Ollivier, V.; Sebbag, U.; Meilhac, O.; Michel, J. B. Involvement of intraplaque hemorrhage in atherothrombosis evolution via neutrophil protease enrichment. *J. Leukocyte Biol.* **2007**, *82*, 1420–1429.

(22) Leclercq, A.; Houard, X.; Loyau, S.; Philippe, M.; Sebbag, U.; Meilhac, O.; Michel, J. B. Topology of protease activities reflects atherothrombotic plaque complexity. *Atherosclerosis* **2007**, *191*, 1–10.

(23) Le Dall, J.; Ho-Tin-Noé, B.; Louedec, L.; Meilhac, O.; Roncal, C.; Carmeliet, P.; Germain, S.; Michel, J. B.; Houard, X. Immaturity of microvessels in haemorrhagic plaques is associated with proteolytic degradation of angiogenic factors. *Cardiovasc. Res.* **2010**, *85*, 184–193.

(24) Stary, H. C.; Chandler, A. B.; Dinsmore, R. E.; Fuster, V.; Glagov, S.; Insull, W.; Rosenfeld, M. E.; Schwartz, C. J.; Wagner, W. D.; Wissler, R. W. A definition of advanced types of atherosclerotic lesions and a histological classification of atherosclerosis. A report from the Committee on Vascular Lesions of the Council on Arteriosclerosis, American Heart Association. *Arterioscler., Thromb., Vasc. Biol.* **1995**, *15*, 1512–1531.

(25) Hyafil, F.; Laissy, J. P.; Mazighi, M.; Tchétché, D.; Louedec, L.; Adle-Biassette, H.; Chillon, S.; Henin, D.; Jacob, M. P.; Letourneur, D.; Feldman, L. J. Ferumoxtran-10-enhanced MRI of the hyper-cholesterolemic rabbit aorta: relationship loss and macrophage infiltration. *Arterioscler., Thromb., Vasc. Biol.* **2006**, *26*, 176–181.

(26) Galis, Z. S.; Sukhova, G. K.; Lark, M. W.; Libby, P. Increased expression of matrix metalloproteinases and matrix degrading activity in vulnerable regions of human atherosclerotic plaques. *J. Clin. Invest.* **1994**, *94*, 2493−2503.

(27) Galis, Z. S.; Sukhova, G. K.; Libby, P. Microscopic localization of active proteases by in situ zymography: detection of matrix metalloproteinase activity in vascular tissue. *FASEB J.* **1995**, *9*, 974−980.

(28) Li, Z.; Li, L.; Zielke, H. R.; Cheng, L.; Xiao, R.; Crow, M. T.; Stetler-Stevenson, W. G.; Froehlich, J.; Lakatta, E. G. Increased expression of 72-kd type IV collagenase (MMP-2) in human aortic atherosclerotic lesions. *Am. J. Pathol.* **1996**, *148*, 121−128.

(29) Halpert, I.; Sires, U. I.; Roby, J. D.; Potter-Perigo, S.; Wight, T. N.; Shapiro, S. D.; Welgus, H. G.; Wickline, S. A.; Parks, W. C. Matrilysin is expressed by lipid-laden macrophages at sites of potential rupture in atherosclerotic lesions and localizes to areas of versican deposition, a proteoglycan substrate for the enzyme. *Proc. Natl. Acad. Sci.* **1996**, *93*, 9748−9753.

(30) Schönbeck, U.; Mach, F.; Sukhova, G. K.; Atkinson, E.; Levesque, E.; Herman, M.; Graber, P.; Basset, P.; Libby, P. Expression of stromelysin-3 in atherosclerotic lesions: regulation via CD40-CD40 ligand signaling in vitro and in vivo. *J. Exp. Med.* **1999**, *189*, 843−853.

(31) Sukhova, G. K.; Schönbeck, U.; Rabkin, E.; Schoen, F. J.; Poole, A. R.; Billinghurst, R. C.; Libby, P. Evidence for increased collagenolysis by interstitial collagenases-1 and -3 in vulnerable human atheromatous plaques. *Circulation* **1999**, *99*, 2503−2509.

(32) Rajavashisth, T. B.; Xu, X. P.; Jovinge, S.; Meisel, S.; Xu, X. O.; Chai, N. N.; Fishbein, M. C.; Kaul, S.; Cercek, B.; Sharifi, B.; Shah, P. K. Membrane type 1 matrix metalloproteinase expression in human atherosclerotic plaques: evidence for activation by proinflammatory mediators. *Circulation* **1999**, *99*, 3103−3109.

(33) Uzui, H.; Harpf, A.; Liu, M.; Doherty, T. M.; Shukla, A.; Chai, N. N.; Tripathi, P. V.; Jovinge, S.; Wilkin, D. J.; Asotra, K.; Shah, P. K.; Rajavashisth, T. B. Increased expression of membrane type 3-matrix metalloproteinase in human atherosclerotic plaque: role of activated macrophages and inflammatory cytokines. *Circulation* **2002**, *106*, 3024−3030.

(34) Herman, M. P.; Sukhova, G. K.; Libby, P.; Gerdes, N.; Tang, N.; Horton, D. B.; Kilbride, M.; Breitbart, R. E.; Chun, M.; Schönbeck, U. Expression of neutrophil collagenase (matrix metalloproteinase-8) in human atheroma: a novel collagenolytic pathway suggested by transcriptional profiling. *Circulation* **2001**, *104*, 1899−1904.

(35) Dollery, C. M.; Owen, C. A.; Sukhova, G. K.; Krettek, A.; Shapiro, S. D.; Libby, P. Neutrophil elastase in human atherosclerotic plaques: production by macrophages. *Circulation* **2003**, *107*, 2829−2836.

(36) Ribichini, F.; Pugno, F.; Ferrero, V.; Bussolati, G.; Feola, M.; Russo, P.; Di Mario, C.; Colombo, A.; Vassanelli, C. Cellular immunostaining of angiotensin-converting enzyme in human coronary atherosclerotic plaques. *J. Am. Coll. Cardiol.* **2006**, *47*, 1143−1149.

(37) Diet, F.; Pratt, R. E.; Berry, G. J.; Momose, N.; Gibbons, G. H.; Dzau, V. J. Increased accumulation of tissue ACE in human atherosclerotic coronary artery disease. *Circulation* **1996**, *94*, 2756−2767.

(38) Fukuhara, M.; Geary, R. L.; Diz, D. I.; Gallagher, P. E.; Wilson, J. A.; Glazier, S. S.; Dean, R. H.; Ferrario, C. M. Angiotensin-converting enzyme expression in human carotid artery atherosclerosis. *Hypertension* **2000**, *35*, 353−359.

(39) Schieffer, B.; Schieffer, E.; Hilfiker-Kleiner, D.; Hilfiker, A.; Kovanen, P. T.; Kaartinen, M.; Nussberger, J.; Harringer, W.; Drexler, H. Expression of angiotensin II and interleukin 6 in human coronary atherosclerotic plaques: potential implications for inflammation and plaque instability. *Circulation* **2000**, *101*, 1372−1378.

(40) Zulli, A.; Burrell, L. M.; Widdop, R. E.; Black, M. J.; Buxton, B. F.; Hare, D. L. Immunolocalization of ACE2 and AT2 receptors in rabbit atherosclerotic plaques. *J. Histochem. Cytochem.* **2006**, *54*, 147−150.

(41) Le Guen, S.; Mas Nieto, M.; Canestrelli, C.; Chen, H.; Fournie-Zaluski, M. C.; Cupo, A.; Maldonado, R.; Roques, B. P.; Noble, F. Pain management by a new series of dual inhibitors of enkephalin degrading enzymes: long lasting antinociceptive properties and potentiation by CCK2 antagonist or methadone. *Pain* **2003**, *104*, 139−148.

(42) Yamamoto, N.; Nakayama, J.; Yamakawa-Kobayashi, K.; Hamaguchi, H.; Miyazaki, R.; Arinami, T. Identification of 33 polymorphisms in the adipocyte-derived leucine aminopeptidase (ALAP) gene and possible association with hypertension. *Hum. Mutat.* **2002**, *19*, 251−257.

(43) Minamino, T.; Kurihara, H.; Takahashi.; et al. Endothelin-converting enzyme expression in the rat vascular injury model and human coronary atherosclerosis. *Circulation* **1997**, *95*, 221−230.

(44) Maguire, J.; Davenport, A. Increased response to big endothelin-1 in atherosclerotic human coronary artery: functional evidence for up-regulation of endothelin-converting enzyme activity in disease. *Br. J. Pharmacol.* **1998**, *125*, 238−240.

(45) Hai, E.; Ikura, Y.; Naruko, T.; Shirai, N.; Yoshimi, N.; Kayo, S.; Sugama, Y.; Fujino, H.; Ohsawa, M.; Tanzawa, K.; Yokota, T.; Ueda, M. Alterations of endothelin-converting enzyme expression in early and advanced stages of human coronary atherosclerosis. *Int. J. Mol. Med.* **2004**, *13*, 649−654.

(46) Hyafil, F.; Vucic, E.; Cornily, J. C.; Sharma, R.; Amirbekian, V.; Blackwell, F.; Lancelot, E.; Corot, C.; Fuster, V.; Galis, Z. S.; Feldman, L. J.; Fayad, Z. A. Monitoring of arterial wall remodelling in atherosclerotic rabbits with a magnetic resonance imaging contrast agent binding to matrix metalloproteinases. *Eur. Heart J.* **2011**, *32*, 1561−1571.

(47) de Smet, B. J.; de Kleijn, D.; Hanemaaijer, R.; Verheijen, J. H.; Robertus, L.; van Der Helm, Y. J.; Borst, C.; Post, M. J. Metalloproteinase inhibition reduces constrictive arterial remodeling after balloon angioplasty: a study in the atherosclerotic Yucatan micropig. *Circulation* **2000**, *101*, 2962−2967.

(48) Schafers, M.; Riemann, B.; Kopka, K.; Breyholz, H. J.; Wagner, S.; Schafers, K. P.; Law, M. P.; Schober, O.; Levkau, B. Scintigraphic imaging of matrix metalloproteinase activity in the arterial wall in vivo. *Circulation* **2004**, *109*, 2554−2559.